

Contraction of the Northern Hemisphere, Lower-Tropospheric, Wintertime Cold Pool over the Past 66 Years

JONATHAN E. MARTIN

Department of Atmospheric and Oceanic Sciences, University of Wisconsin–Madison, Madison, Wisconsin

(Manuscript received 17 July 2014, in final form 29 January 2015)

ABSTRACT

Employing reanalysis datasets, several threshold temperatures at 850 hPa are used to measure the wintertime [December–February (DJF)] areal extent of the lower-tropospheric, Northern Hemisphere, cold-air pool over the past 66 cold seasons. The analysis indicates a systematic contraction of the cold pool at each of the threshold temperatures. Special emphasis is placed on analysis of the trends in the extent of the -5°C air.

Composite differences in lower-tropospheric temperature, midtropospheric geopotential height, and tropopause level jet anomalies between the five coldest and five warmest years are considered. Cold years are characterized by an equatorward expansion of the jet in the Pacific and Atlantic sectors of the hemisphere and by invigorated cold-air production in high-latitude Eurasia and North America. Systematic poleward encroachment of the -5°C isotherm in the exit regions of the storm tracks accounts for nearly 50% of the observed contraction of the hemispheric wintertime cold pool since 1948. It is suggested that this trend is linked to displacement of the storm tracks associated with global warming.

Correlation analyses suggest that the interannual variability of the areal extent of the 850-hPa cold pool is unrelated to variations in hemispheric snow cover, the Arctic Oscillation, or the phase and intensity of ENSO. A modest statistical connection with the East Asian winter monsoon, however, does appear to exist. Importantly, there is no evidence that a resurgent trend in cold Northern Hemisphere winters is ongoing. In fact, the winter of 2013/14, though desperately cold in North America, was the warmest ever observed in the 66-yr time series.

1. Introduction

A large variety of in situ and remote measurements point toward a general warming of the planet over the past century and a half (Stocker et al. 2014). Analysis of surface temperature data (e.g., Hansen et al. 2001; Lugina et al. 2005; Smith and Reynolds 2005; Smith et al. 2005; Brohan et al. 2006; Hansen et al. 2010), various measures of the extent and age of Arctic sea ice (e.g., Serreze et al. 2007), decreased snow cover in many Northern Hemisphere (NH) locations (Brown 2000), as well as the length of ice duration on lakes and rivers across the Northern Hemisphere (Magnuson et al. 2000) are among the various pieces of evidence that testify to this warming.

Recent advances in the analysis of historic radiosonde and satellite data as manifest in modern reanalysis datasets have revealed a concurrent warming of the

lower troposphere (Karl et al. 2006). Although upper-air datasets have been subjected to less scrutiny than surface datasets and adjustments to the raw data are complicated and dependent upon expert judgment, it is considered very likely that these estimates give reliable indications of the direction of lower-tropospheric temperature change over the last half-century. Nonetheless, free tropospheric temperature measurements are still considered among the least confident metrics of climate change (Stocker et al. 2014).

Despite this varied and increasingly refined evidence, the relatively small amount of uncertainty that remains is apparently sufficient to maintain public skepticism regarding global warming at a disproportionately high level (Scruggs and Benegal 2012). In this paper, we introduce a novel analysis of lower-tropospheric wintertime temperature trends by employing a number of long-term, 4-times daily reanalysis datasets in order to compute the area, at mid- and high latitudes, covered by air colder than a series of threshold temperatures at 850 hPa. Calculation of the hemispheric area of what we term the 850-hPa cold pool eliminates regional bias from

Corresponding author address: Department of Atmospheric and Oceanic Sciences, University of Wisconsin–Madison, 1225 W. Dayton Street, Madison, WI 53706.
E-mail: jemarti1@wisc.edu

the analysis of long-term trends in lower-tropospheric temperature and better testifies to the intensity of the cold season over the entire hemisphere and the variation of that intensity from year to year. Additionally, the modest to substantial averaging employed to generate elements of the foregoing analysis may mitigate some of the uncertainties inherent in the reanalysis products themselves. The cold pool area is extremely simple to calculate, and analysis of the results reveals a number of trends consistent with a gradual warming of the troposphere over the last 66 yr. The present paper considers aspects of both the long-term, seasonally averaged trend in the areal extent of the 850-hPa cold pool as well as its interannual variability.

The paper is organized in several sections: [Section 2](#) provides a description of the methodology used in calculating the cold pool area as well as a description of the reanalysis datasets employed in the analysis. In [section 3](#), aspects of the long-term trend and interannual variability of this measure of winter severity are considered. Included here is an analysis of the geographic distribution of the variability of the areal extent of the 850-hPa cold pool as well as an analysis of differences in the composite, large-scale thermodynamic and kinematic structures exhibited by the coldest and warmest years. Finally, examination of the temperature distribution and first-order characteristics of extreme events are considered in [section 4](#). A summary and conclusions, including suggestions for future work, are offered in [section 5](#).

2. Data and methodology

To demonstrate the robustness of the results, the study employs three distinct reanalysis datasets: the National Centers for Environmental Prediction–National Center for Atmospheric Research (NCEP–NCAR) reanalysis, ERA-40, and the NCEP Climate Forecast System Reanalysis (CFSR). Both the NCEP–NCAR reanalysis ([Kalnay et al. 1996](#)) and ERA-40 ([Uppala et al. 2005](#)) employ relatively large grid spacing ($2.5^\circ \times 2.5^\circ$). The NCEP–NCAR reanalysis derives from a frozen state-of-the-art global assimilation system in conjunction with a database that includes in situ and remotely sensed data (when available) both at the surface and at levels through the troposphere and stratosphere. The present study employs data spanning the period 1 January 1948–28 February 2014. ERA-40 is a reanalysis of a variety of in situ and remote meteorological observations spanning the period 1 September 1957–31 August 2002. NCEP's CFSR data ([Saha et al. 2010](#)) is a high-resolution ($0.5^\circ \times 0.5^\circ$) reanalysis that includes all available conventional and satellite observations. In this study, CFSR data from 1 January 1979 to 31 December 2010 are considered.

(More details on this dataset can be found at <http://cfs.ncep.noaa.gov/cfsr>.)

In each of these reanalysis datasets, gridded data are available daily at 0000, 0600, 1200, and 1800 UTC. At each of these times the areal extent of the -5° , -10° , -15° , -20° , and -25°C air at 850 hPa in the Northern Hemisphere in the months of December–February (boreal winter, skipping leap days) is considered. The 850-hPa level is chosen as it is high enough to be above the wintertime boundary layer at low elevation locations but low enough to be safely considered as lower tropospheric. The method of calculation is identical for all of the datasets employed in this study. The total hemispheric area occupied by air colder than each threshold at each time is the sum of the areas so occupied in each grid box and is exact at the resolution of the dataset.

Much of the subsequent analysis will emphasize characteristics of the seasonal and daily areal extent of the -5°C air at 850 hPa. This choice is motivated by two primary considerations. First, since -5°C at 850 hPa is often a reliable discriminator between liquid and frozen precipitation in midlatitude winter storms, it is a synoptically familiar and operationally relevant value. Second, -5°C is often embedded within the frontal zones of all but the weakest winter storms and so is subject to substantial deformation by both horizontal and vertical advection. Though such advectations may influence the day-to-day variability of the areal extent of such air, neither type of advection can systematically create or destroy cold air. Thus, the fact that -5°C air at 850 hPa often extends deep into the midlatitudes makes it particularly illustrative of the fact that the expansion or contraction of the 850-hPa cold pool over a long time series testifies to changes in radiative forcing over the same period.

The analysis begins by presenting seasonally averaged 850-hPa cold pool areas for each of the last 66 Northern Hemisphere winters [December–February (DJF)] at five different threshold temperatures. Characteristics of the daily averaged values over this time period are considered subsequently.

3. Results

a. Seasonally averaged trends

The 66-season time series of Northern Hemisphere, seasonally averaged,¹ 850-hPa cold pool area at five different threshold temperatures is shown in [Fig. 1](#). A number of important features characterize the time series and

¹ The average area for a given season is the mean of the 360 6-h areas calculated from 1 December to 28 February in that cold season.

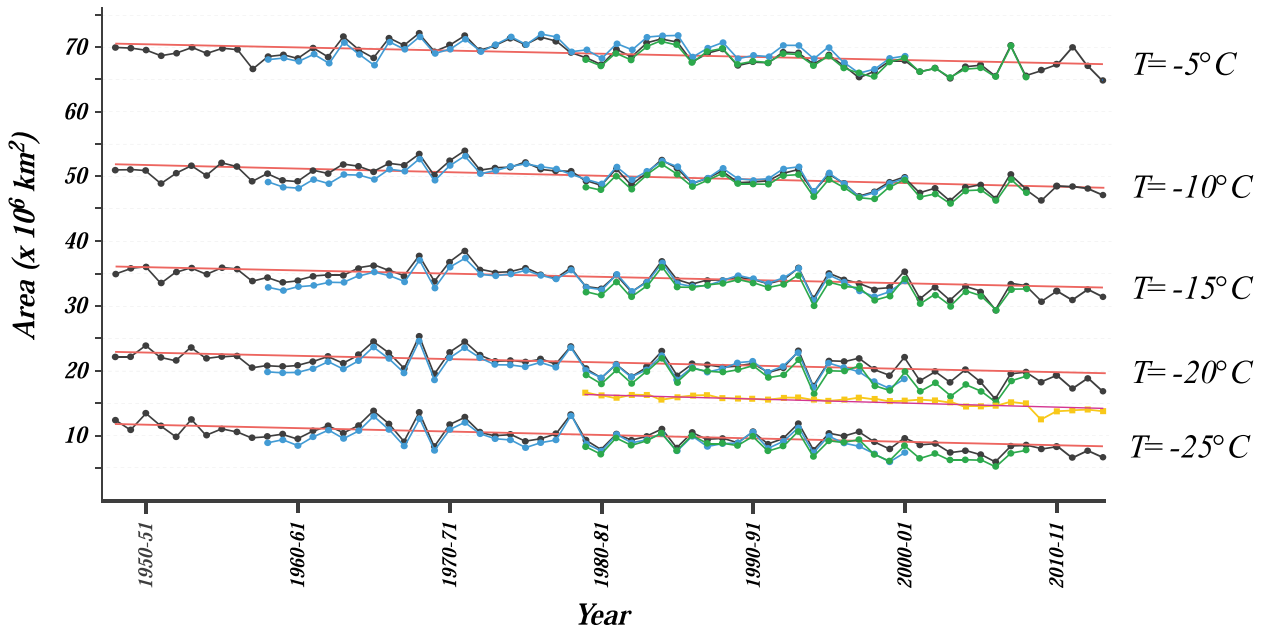


FIG. 1. Time series of seasonally averaged areal extent of 850-hPa cold pool at five indicated threshold temperatures. Black line with black dots is the 66-yr time series derived from the NCEP reanalysis data. Blue line with blue dots is the 44-yr time series derived from the ERA-40 data. Green line with green dots is the 30-yr time series derived from the NCEP CFSR data. Red lines represent the trend lines (significant at the 99.9% level) calculated using the NCEP reanalysis time series. Orange line with squares is the 30-yr time series of February sea ice extent with magenta line indicating the trend (significant at the 99.9% level).

are worthy of note. First, the areal extent of the Northern Hemisphere wintertime cold pool at 850 hPa has systematically decreased over this interval at all five threshold temperatures. Specifically, the decreases² have been 4.74%, 7.11%, 10.24%, 17.71%, and 33.86% at -5° , -10° , -15° , -20° , and -25°C , respectively. For each threshold temperature, a linear least squares trend line was fit to the seasonally averaged data. In each case, the trend line is statistically significant above the 99.9% level.

The linearly decreasing trends identified in the NCEP–NCAR data are also identified in the CFSR data (green dots in Fig. 1). Despite the substantially smaller grid spacing of the CFSR data, the seasonally averaged areas are nearly identical to those calculated using the NCEP–NCAR data, especially at -5° and -10°C . At colder threshold temperatures, the areas calculated using the CFSR data are smaller, but the trends are identical. Similar departures from near-perfect agreement between the NCEP–NCAR and ERA-40 data (blue dots in Fig. 1) occur at colder threshold temperatures. These departures from the NCEP–NCAR data are largest from 1997/98 to 2005/06 (2000/01 for ERA-40). It is notable that during these seasons, the CSFR and ERA-40 data

are in close agreement at these colder thresholds. Given its longer time series and the general agreement among the various datasets with regard to the areal extent of the cold air, subsequent analyses will exclusively employ the NCEP reanalysis dataset.

Also included in Fig. 1, and scaled to fit the ordinate axis, is the time series of February Arctic sea ice extent since 1979 (Serreze et al. 2007). The year-to-year variability of the time series on this scale is smaller than that of the cold pool area variability, but the slope of the trend line is very similar to the set of slopes represented by the five thresholds. Thus, it appears that the late winter extent of the Arctic sea ice has decreased at a rate similar to the shrinking of the lower-tropospheric wintertime cold pool.

Another perspective on the seasonally averaged time series of the 850-hPa cold pool is afforded by Fig. 2, which portrays the time series of the areal extent of -5°C air in terms of normalized area.³ Only 12 of the 43 winter seasons before 1990/91 had below average, seasonally averaged areas, whereas 20 of 24 winter seasons have had below average, seasonally averaged areas since. Notably, the winter of 2013/14, notorious for

² The percentage decrease is measured using the linear trend line as $[(\text{Area}_{48-49} - \text{Area}_{13-14})/\text{Area}_{48-49}] \times 100\%$.

³ The mean and standard deviation used to normalize these data are those derived from the full 66-yr NCEP reanalysis time series.

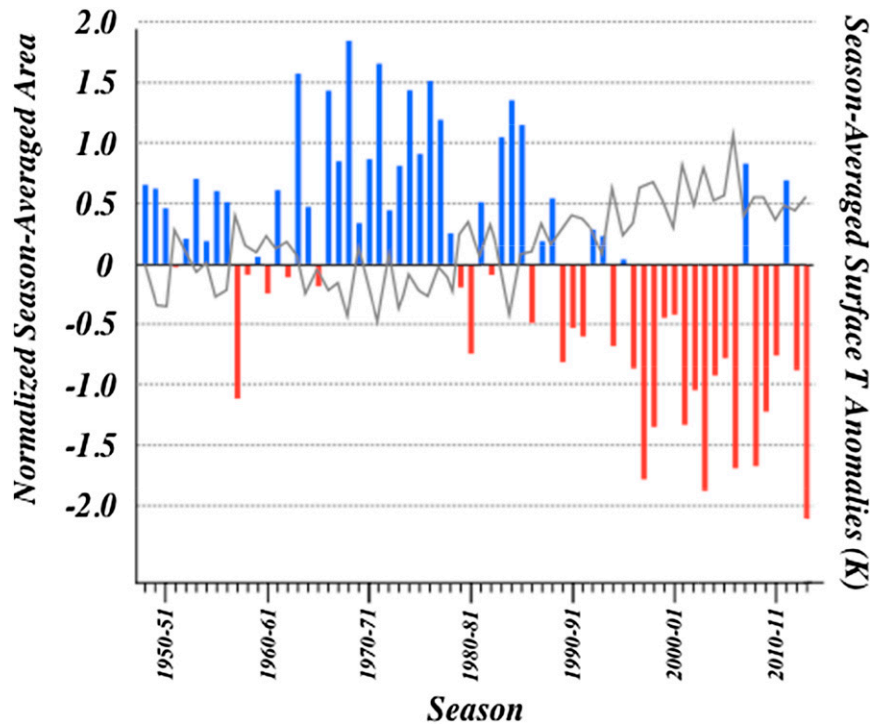


FIG. 2. Time series of normalized DJF-averaged areal extent of the -5°C air at 850 hPa. Blue (red) bars represent the extent above (below) average seasonally averaged area for a given season. Solid gray line is the DJF-averaged Northern Hemisphere surface temperature anomaly (from the 1961–90 average) from the HadCRUT4 data (Morice et al. 2012). The two time series are correlated at $-0.833\ 37$. Similar correlations exist for the GISTEMP ($r = 0.833\ 55$) and NOAA GHCN-M, version 3 ($r = 0.837\ 10$), temperature anomaly datasets.

the persistent nature of the cold it dealt to North America, was the “warmest” season, hemispherically, in the entire 66-yr time series.

The relationship between the areal extent of the 850-hPa cold pool and Northern Hemisphere surface temperature anomalies was explored using three surface temperature datasets: the GISTEMP (Hansen et al. 2010), NOAA’s Global Historical Climatology Network–monthly mean (GHCN-M), version 3 (Lawrimore et al. 2011), and the Hadley Centre’s HadCRUT4 dataset (Morice et al. 2012). Since only minor differences exist among these different datasets, only the most poorly correlated time series, the HadCRUT4 ($r = -0.833\ 37$), is illustrated in Fig. 2. The explained variance between the areal extent of the 850-hPa, wintertime cold pool and Northern Hemisphere average surface temperature is more than 69% for all three datasets.

Averaging the 66 daily average areas, at each threshold temperature, for a given calendar day renders the average areal extent for that threshold temperature for that calendar day. Figure 3 shows the resulting annual cycle for each of the five chosen threshold temperatures at 850 hPa. Interestingly, the warmer threshold temperatures reach

peak areal extent approximately two weeks later than the colder temperatures (-20° and -25°C).

Insight into the geographical variability of the cold pool arises by considering the 66-yr time series of the seasonally averaged latitude of the -5°C isotherm around the globe. The DJF-averaged position of the -5°C isotherm is shown in Fig. 4. The analysis clearly suggests that the continental regions of Eurasia–Siberia and Canada serve as the two foci for cold-air production/anchoring during Northern Hemisphere winter. Adding the $\pm 1\sigma$ bounds to the average latitude demonstrates that not all regions of the hemisphere are as likely to contribute to an abnormally cold or warm winter as others (Fig. 4). Notably, the entrance regions of both the Pacific and Atlantic storm tracks are among the least variable locations, whereas regions downstream of the storm tracks are among the most variable. These inferences are further supported by consideration of the distribution of the seasonally averaged extreme latitudes at each longitude (Fig. 4). Particularly prone to a wide range of seasonal extremes is Scandinavia and northwestern Europe with an elongated secondary zone of variability extending from just east of Japan to the Great Lakes of North America.

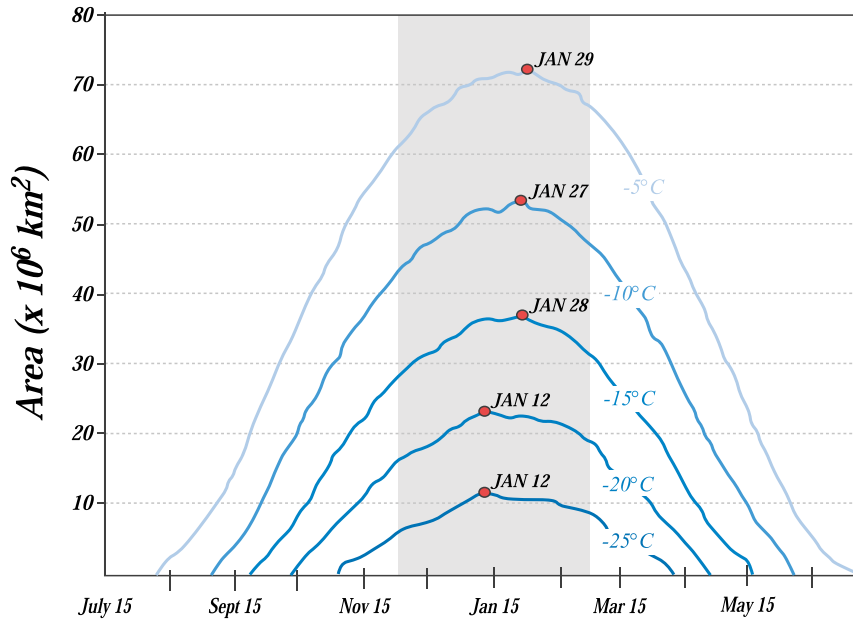


FIG. 3. Daily averaged area of 850-hPa cold pool at five threshold temperatures derived from 66 yr of NCEP reanalysis data. Gray shading identifies 1 Dec–28 Feb and indicated calendar dates correspond to the day of peak extent of the 850-hPa cold pool at the indicated threshold.

A linear trend line of the seasonally averaged latitude of the -5°C isotherm was calculated for each 10° increment of longitude. Only three longitude sectors around the hemisphere exhibit trends in the average latitude of the -5°C isotherm that are significant at or above the 95% level. Two such regions are located at the ends of the Pacific and Atlantic storm tracks (labeled as A and B, respectively, in Fig. 4). At the end of the Pacific storm track, the -5°C isotherm has moved poleward by $\sim 3.13^{\circ}\text{C}^4$ over the 66-yr time series (Fig. 5a). This poleward excursion reduces the areal extent of the cold pool by $8.7193 \times 10^{11} \text{ m}^2$ in this sector that represents over 27% of the observed hemispheric contraction of the -5°C cold pool area over this period. At the end of the Atlantic storm track, the -5°C isotherm has shifted $\sim 3.35^{\circ}$ poleward over the 66-yr time series (Fig. 5b), accounting for nearly 23% ($7.5455 \times 10^{11} \text{ m}^2$) of the observed contraction of the -5°C cold pool over that interval.⁵ Thus, nearly $1/2$ of the observed contraction has systematically taken place in limited longitudinal sectors of the exit regions of the main storm tracks that

characterize Northern Hemisphere winter.⁶ These exit regions are, broadly, the locations of maximum poleward excursion for extratropical cyclones. Given the consensus view that a poleward shift of the midlatitude storm tracks will likely be a leading characteristic of a warmer world (e.g., Wang et al. 2006; Wu et al. 2010), the regional contraction of the cold pool in these areas may be, in part, a manifestation of larger-scale circulation anomalies born of a changing climate.

b. Interannual variability of the cold pool area

Examination of the daily average areas during each cold season demonstrates that despite the systematic, long-term decrease in the seasonally averaged areal extent of the 850-hPa cold pool, there is substantial interannual variability. Figure 6 provides an illustrative example of this variability by overlaying the daily time series of the areal extent of the -5°C air for DJF 2011/12 and 2013/14. Ranking the Northern Hemisphere winter seasons in the time series from “coldest” to “warmest” is accomplished by using the normalized, season-averaged areas portrayed in Fig. 2. By this measure, four of the five coldest winters since 1948/49 occurred

⁴ This value represents the mean of the latitudinal displacements at each longitude in the sector as measured using each longitude’s trend line.

⁵ Region C in Fig. 4 has experienced $\sim 1.76^{\circ}$ poleward shift of the -5°C isotherm since 1948/49, accounting for 5% of the observed contraction of the cold pool.

⁶ The greater latitudinal change in the Atlantic sector corresponds to a smaller area change because the original latitude of the -5°C isotherm there is higher than in the Pacific sector.

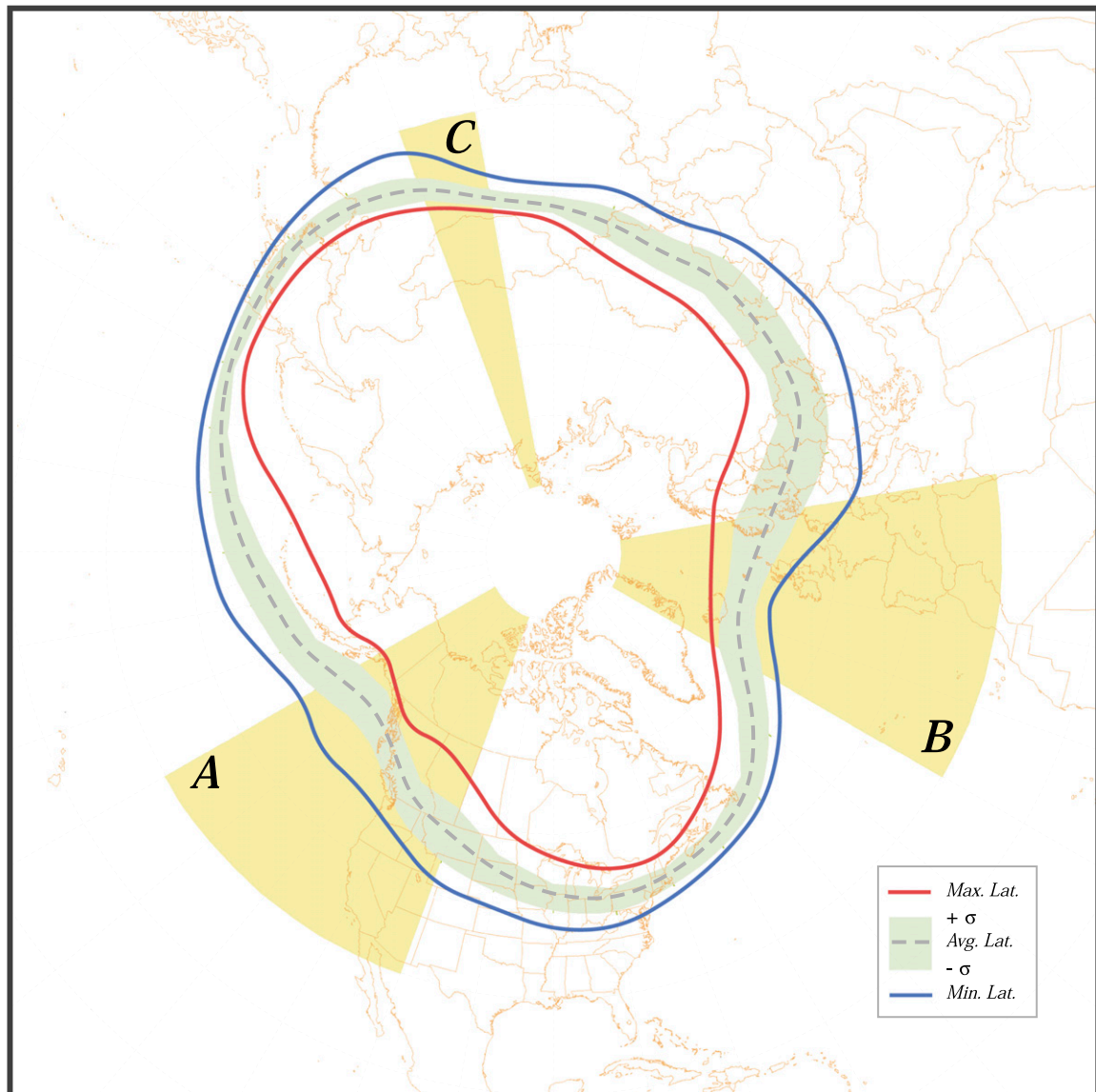


FIG. 4. The 66-yr average DJF latitude (dashed line) of the -5°C isotherm at 850 hPa from the NCEP reanalysis data. Gray shading indicates $\pm 1\sigma$ from that average, while the solid blue (red) line represents the minimum (maximum) latitude of the -5°C isotherm at each longitude over the time series. Yellow shaded regions are regions in which the trend in latitude over the 66-yr time series is significant above the 95% level. See text for explanation. The labels A and B are referenced in Fig. 5.

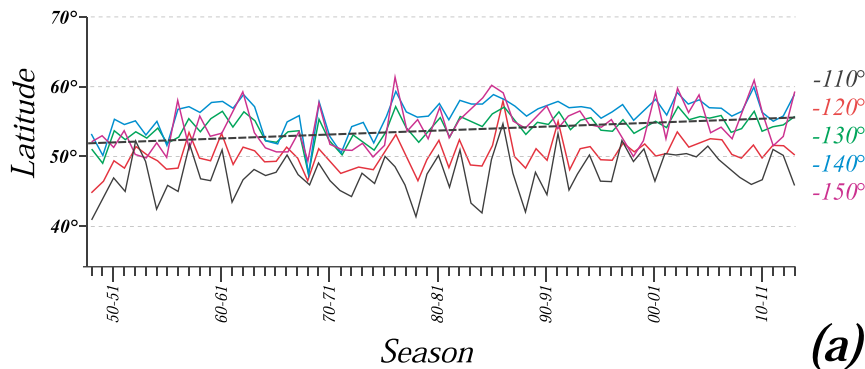
within the 7-yr period from 1968/69 to 1974/75 while four of the five warmest years have occurred since 2003/04.

The composite daily time series of areal extent of the -5°C air at 850 hPa for the five coldest and five warmest years is shown in Fig. 7. During the coldest years, the daily areal extent fluctuates around the $+1\sigma$ value throughout the composite season. The composite daily time series of the warmest years similarly fluctuates around the -1σ value throughout the season. The fact that the warmest years are characterized by larger departures from average than the coldest years (evident

from Fig. 2) is manifest in Fig. 7 by the fact that the red shaded area (representing the integrated daily average departure from -1σ for the warm seasons) exceeds the blue shaded area (conversely defined for the cold seasons) for the composite season.

Construction of a variety of composites of the five coldest and five warmest years lends insight into the differences in DJF hemispheric flow and thermal structure characterizing these extremes. Perhaps unsurprisingly, the composite coldest years are substantially colder in Eurasia–Siberia, as well as in western North America,

Eastern Pacific Region (A)



Eastern Atlantic Region (B)

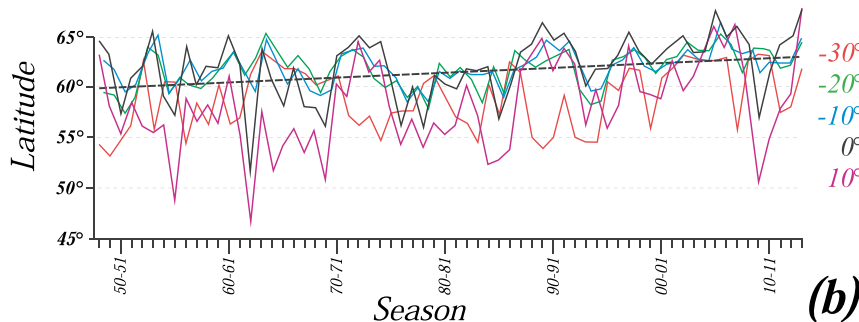


FIG. 5. The 66-yr time series of the DJF average latitude of the -5°C isotherm at 850 hPa from the NCEP reanalysis at selected longitudes for the (a) eastern Pacific region (labeled A in Fig. 4) and (b) the eastern Atlantic region (labeled B in Fig. 4). The dashed black line in (a) and (b) represents the trend line significant above the 95% level.

than the warmest years (Fig. 8a). The abnormal lower-tropospheric cold that characterizes these locations in cold years is reflected in midtropospheric troughing there, while anomalous ridging prevails in the North Atlantic eastward along the Arctic coast of Russia (Fig. 8b), presumably reflecting the relative, lower-tropospheric warmth in the Arctic that characterizes cold years. The resulting meridionally oriented couplet of height perturbations in the North Atlantic–Arctic region is characteristic of the negative phase of the Arctic Oscillation (AO) (Thompson and Wallace 1998). The associated difference field in the 300-hPa wind speeds (Fig. 8c) illustrates that cold years are characterized by a weakened North Atlantic and North Pacific jet stream. In fact, the difference fields can be interpreted as manifestations of an equatorward displacement of the jet core in both the Atlantic and Pacific sectors. Since the jet is dynamically tied to the equatorward edge of the cold air, such

a southward shift over so large a portion of the hemisphere would be consistent with an increased areal extent of the lower-tropospheric cold pool.

It is reasonable to suspect that a number of variable circumstances and/or hemispheric circulation anomalies may exert a discernible influence on the interannual variability of the lower-tropospheric cold pool area. Given the intraseasonal dependence of cold pool expansion and contraction on radiative processes, one might expect that interannual Northern Hemispheric snow cover variations play a substantial role. Indeed, prior studies by Foster et al. (1983) and Cohen and Entekhabi (1999) have explored this connection in detail. Employing the hemispheric snow cover dataset from the Rutgers Global Snow Laboratory (<http://climate.rutgers.edu/snowcover>), the correlation between the DJF average Northern Hemisphere snow cover and the areal extent of the 850-hPa cold pool is

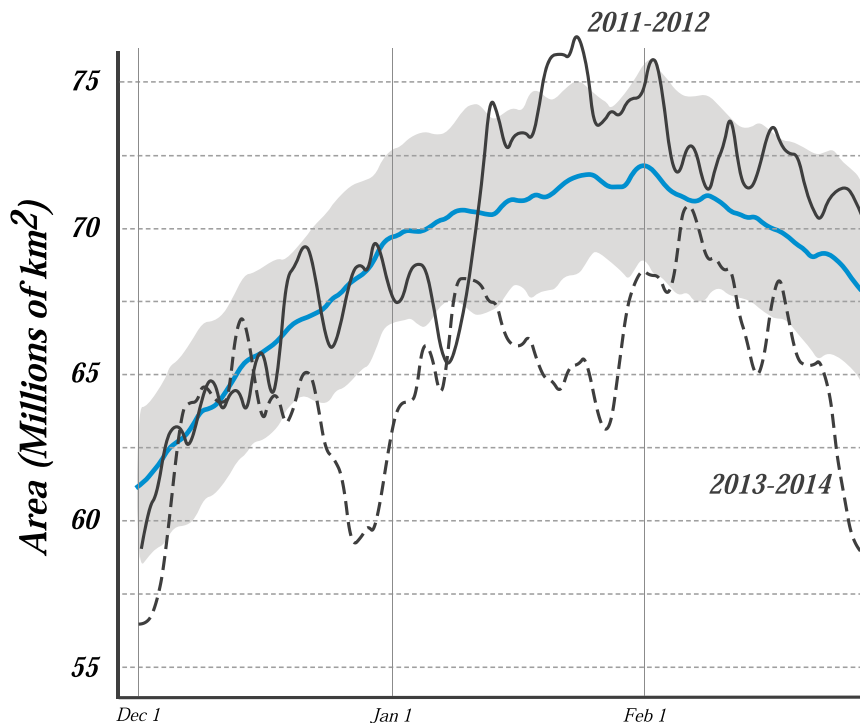


FIG. 6. Daily averaged areal extent of -5°C area at 850 hPa for DJF (1 Dec–28 Feb) in 2011/12 (solid black line) and 2013/14 (dashed black line). Thick blue line represents the 66-yr daily averaged area over DJF from the NCEP reanalysis data. Gray shading indicates the $\pm 1\sigma$ of the daily average area.

0.196, suggesting a fairly meager physical connection. Upon partitioning the cold pool area into separate overland and overocean components, however, the correlations are 0.4327 and -0.2717 , respectively. Lag correlations of the DJF 850-hPa cold pool area with October–November snow cover are also extremely low (0.106; 0.2000 and -0.0958 for overland and overocean, respectively), suggesting that early season snowfall, though potentially important for shaping the regional complexion of the coming winter's lower-tropospheric temperature, has little bearing on the overall hemispheric picture.

By shifting equatorial convection eastward in the Pacific basin, El Niño (the warm phase of ENSO) can have a dramatic effect on the seasonal characteristics of the Pacific jet. In fact, in El Niño years the Pacific jet is often zonally extended to well east of the date line (Chu et al. 1993), consistent with the positive 300-hPa zonal wind speed differences highlighted there in Fig. 8. So, it is plausible that the intensity and phase of ENSO might have a bearing on the interannual variability of the areal extent of the 850-hPa cold pool. The extremely low correlation (-0.101 in December–January and -0.020 in January–February) between the cold pool area and the time series of the multivariate ENSO index (MEI;

Wolter and Timlin 1993) suggests that a systematic connection does not exist.

A similarly low correlation (-0.078) between the seasonally averaged -5°C cold pool area and the seasonally averaged AO index⁷ suggests that the intensity (and waviness) of the North Atlantic jet also does not systematically influence the wintertime expansion or contraction of the cold pool. A relationship between 850-hPa cold pool area and the East Asian winter monsoon (EAWM) will be considered after examination of the distribution of cold air that characterizes both extreme cold and extreme warm events.

4. Some characteristics of extreme events

Another means of gaining insight into the variability of the 850-hPa cold pool is to consider the frequency

⁷ Daily AO index values from 1 January 1950 were obtained from the website of the National Weather Service Climate Prediction Center (NOAA/NWS/CPC) (http://www.cpc.ncep.noaa.gov/products/precip/CWlink/daily_ao_index/ao_index.html). Correlations between the seasonally averaged AO index and the seasonally averaged cold pool areas of -10° , -15° , -20° , and -25°C are -0.09 , -0.17 , -0.23 , and -0.22 , respectively.

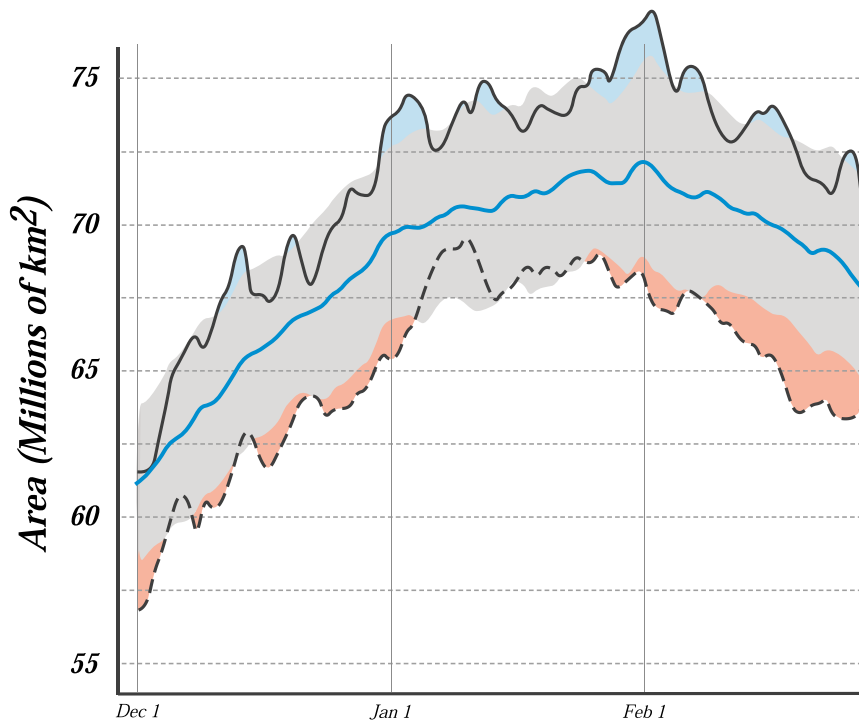


FIG. 7. Daily average areal extent of -5°C air at 850 hPa for the five coldest years (1968/69, 1971/72, 1963/64, 1976/77, and 1974/75, solid black line) and the five warmest years (2013/14, 2003/04, 1997/98, 2006/07, and 2008/09, dashed black line) in the 66-yr NCEP reanalysis time series. Thick blue line is the 66-yr daily average and gray shading indicates the $\pm 1\sigma$ of the daily average area. Light blue (red) shading represents the departure of the cold (warm) days from the daily average $+1\sigma$ (-1σ).

distribution of unusually large and small areas. Days with large (small) areal extent of -5°C air are defined here as those days on which the 850-hPa cold pool area was at least two standard deviations greater than (less than) the mean for that calendar day. Over the course of the 66 winters available, there were 117 (187) days of large (small) area thus defined. Table 1 lists the distribution of each type of event by decade. To the extent that frequent large daily cold pool areas testify to an unusually cold season, it appears that the 1970s was easily the NH's coldest decade in the last half-century, trailed substantially by both the 1960s and the 1980s.⁸ Note that only five large area events have occurred since 1990 and not a single such day has occurred in the last 20 seasons. Of the 187 small area events in the record, more than half (104) have occurred since 2000. In fact, 79.7% of all small area events in the last 66 winters have occurred since 1990. These results are broadly consistent with the observed warming in high latitudes since 1995

(Przybylak 2007) and the fact that the nine warmest years on record (in terms of globally averaged surface temperatures) have occurred in the last 10 yr (NASA GISS).⁹

It is interesting to consider the geographic distribution of the -5°C air at 850 hPa on these extreme cold and warm days. In particular, are there elements of the hemispheric 850-hPa temperature distribution that appear to be characteristic of these extreme winter days? To examine this question, we revisit Table 1 and consider, for example, all the listed December days on which an extreme cold event occurred. In some Decembers more than one day meets the criteria for a cold event (e.g., in December 1948 there were four such days). To eliminate the effect of serial correlation on the foregoing analysis, in such a case only one qualifying day (24 December 1948) in that month was chosen (at random) for comparison against other December days of extreme cold throughout the

⁸ Only two winter seasons from the 1940s are available in the dataset and yet five large area events were recorded in those two seasons.

⁹ This report is available at <http://www.nasa.gov/topics/earth/features/2011-temps.html>.

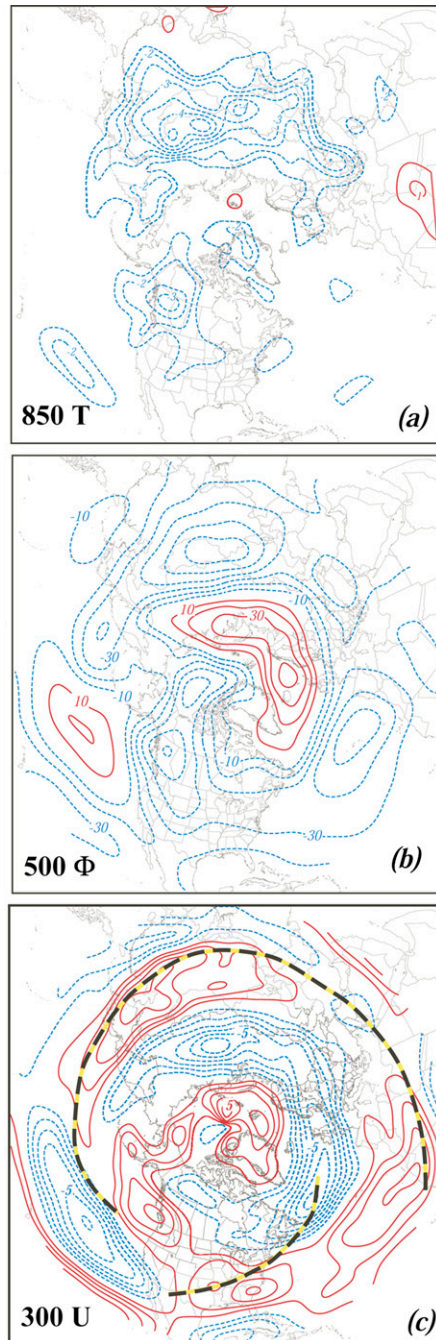


FIG. 8. Difference between the composite five coldest and five warmest winter seasons in terms of (a) 850-hPa temperature (T), (b) 500-hPa geopotential height (ϕ), and (c) 300-hPa zonal wind (U). The 850-hPa T differences [in (a)] labeled in kelvin and contoured every ± 1 K with negative (positive) differences in dashed (solid) blue (red). The 500-hPa ϕ differences [in (b)] labeled in meters and contoured every ± 10 m with negative (positive) differences in dashed (solid) blue (red). The 300-hPa U differences [in (c)] labeled in meters per second and contoured every ± 1 m s^{-1} with negative (positive) differences in dashed (solid) blue (red). Dashed black-yellow line in (c) is the DJF climatological position of the 300-hPa jet axis.

66-yr time series. There were 12 different Decembers in the time series that contained at least one extreme cold event day. The -5°C isotherm from a single qualifying day from each such month is plotted as a blue line in Fig. 9a along with a set of red lines that are the 66-yr average -5°C isotherms for the December calendar days that were selected. A similar subjective filtering was employed to select representative days for each type of extreme event from each month in the dataset. The results of this analysis are shown in Fig. 9.

Overall, the analysis suggests that there are a number of ways in which the -5°C air is distributed around the Northern Hemisphere during an extreme cold or warm event. Despite the fairly substantial amount of variability that exists among extreme events, a few noteworthy common features are evident. For instance, it appears that when the hemisphere is in a $+2\sigma$ cold event, there is a cold surge into central and southern China (a feature that is absent in all but one extreme warm event) suggesting a relationship between the EAWM surge phase and extreme cold events over the entire hemisphere. The China–western Pacific region exhibits little variability during cold events as a systematic, fairly uniform equatorward displacement of the -5°C isotherm relative to its mean position occurs there (Figs. 9a–c). Warm events in this region are also among the least variable in the hemisphere, though the -5°C isotherm is not so uniformly poleward of its mean position (Figs. 9d–f) as its cold counterparts are equatorward.

Though characterized by more variability, the difference between extreme cold and warm events in North America is also quite apparent. This is decidedly not the case for Europe and western Russia where the difference between extreme cold and warm events is nearly indistinguishable, especially in December and January (cf. Figs. 9a,d and 9b,e). Not until February are most of the individual -5°C isotherms portrayed in Fig. 9 in the extreme cold (warm) events finally equatorward (poleward) of their mean positions in that region of the hemisphere.

The ubiquity of the central/southern China cold surge that appears to characterize 2σ cold events motivated additional analysis. Figure 10a shows a map of the correlation between the 66-yr time series of December 850-hPa temperature (T) at each grid point (from 20° to 90°N) in the NCEP reanalysis data with the 66-yr time series of the standardized anomaly of December Northern Hemisphere 850-hPa -5°C cold pool area. The analysis reveals that cold air in central China is correlated with larger than normal areal extent of the hemispheric cold pool. This relationship becomes more robust in January (Fig. 10b) and even more so in February

TABLE 1. List of all calendar dates (DJF) on which the areal extent of the 850-hPa -5°C air (as measured using the NCEP reanalysis data) was observed to be at least 2σ above (below) the 66-yr daily average for that calendar day. The text describes these occurrences as extreme cold ($+2\sigma$) and extreme warm (-2σ) events.

Extreme ($+2\sigma$) cold events	Extreme (-2σ) warm events
1940s (5) 22–25 Dec 1948 12 Dec 1949	1940s (0)
1950s (12) 1–2 Dec 1952 28 Jan 1954 22 Dec, 1–2 and 15–20 Feb 1956	1950s (11) 21 Jan 1950 19 Dec 1954 7 and 11–13 Jan 1956 20 Dec, 27–29 Jan 1958 23 Jan 1959
1960s (25) 1–2 Dec 1964 26–27 and 29 Dec 1966 2–3 and 6–8 Jan, 14 and 22 Feb 1967 31 Dec 1968 1 and 3–7 Jan, 3, 7–8, and 26–28 Feb 1969	1960s (4) 5 Dec 1966 5–7 Dec 1969
1970s (46) 26–27 Dec, 4–7 Jan 1970 26–31 Jan, 1–3 and 7–9 Feb 1972 13 and 19 Dec, 17 Jan, 5 and 24–26 Feb 1974 12–15 Dec 1975 1–2, 9–15, 17, and 31 Jan 1977 9–10 and 14–17 Feb 1978	1970s (9) 4 Dec 1972 15–17 Feb 1974 4–6, 14, and 20 Dec 1979
1980s (24) 29–31 Jan, 4–5 Feb 1980 22 and 28–31 Dec, 18–22 Jan, 6 Feb 1984 1–2 Dec, 1 and 15 Jan 1985 8–10 and 28 Feb 1986	1980s (16) 23–24 Jan 1981 21–22 and 27 Dec, 27–28 Feb 1982 27–28 Jan 1983 4–8, 10–11 Feb 1987
1990s (5) 14–15 Jan, 24 Feb 1993 12–13 Feb 1994	1990s (43) 15 and 18 Dec 1990 15 Dec, 3 and 9–10 Feb 1993 29–30 Dec, 15–16 Feb 1995 14 Jan 1996 17 Dec, 25–26 Feb 1997 13–14 and 16–19 Dec, 12–14 and 16–26 Feb 1998 28 Dec, 18–23 Jan, 13–14 Feb 1999
2000s (0)	2000s (72) 4–12 Jan, 8, 11–12, and 19–20 Feb 2002 1–3, 17–22, and 24–30 Dec, 16–18 and 21 Jan 2003 16 Dec, 19–22 and 24–26 Feb 2004 24–25 Dec 2005 8–13 Dec 2006 1–4 Jan 2007 1–4 and 8 Dec 2008 19–22, 25–26, and 30–31 Jan, 3 and 8–11 Feb 2009
2010s (0)	2010s (32) 7–9, 13–14, and 20 Dec, 14–17 Jan, 27–28 Feb 2010 27–31 Dec, 27–31 Jan, 1 Feb 2013 1, 7, 22–23, and 25–29 Jan 2014

(Fig. 10c) when the strongest correlation reaches -0.52 about 500 km south of Beijing. Thus, there appears to be some relationship between the EAWM and the expansion and contraction of the hemispheric 850-hPa cold pool. Investigation of the physical processes that might compel this association is currently ongoing.

5. Summary and concluding remarks

Employing three different reanalysis datasets, the analysis presented here demonstrates that the 850-hPa wintertime cold pool has systematically contracted, at each of several threshold temperatures, since the mid-twentieth

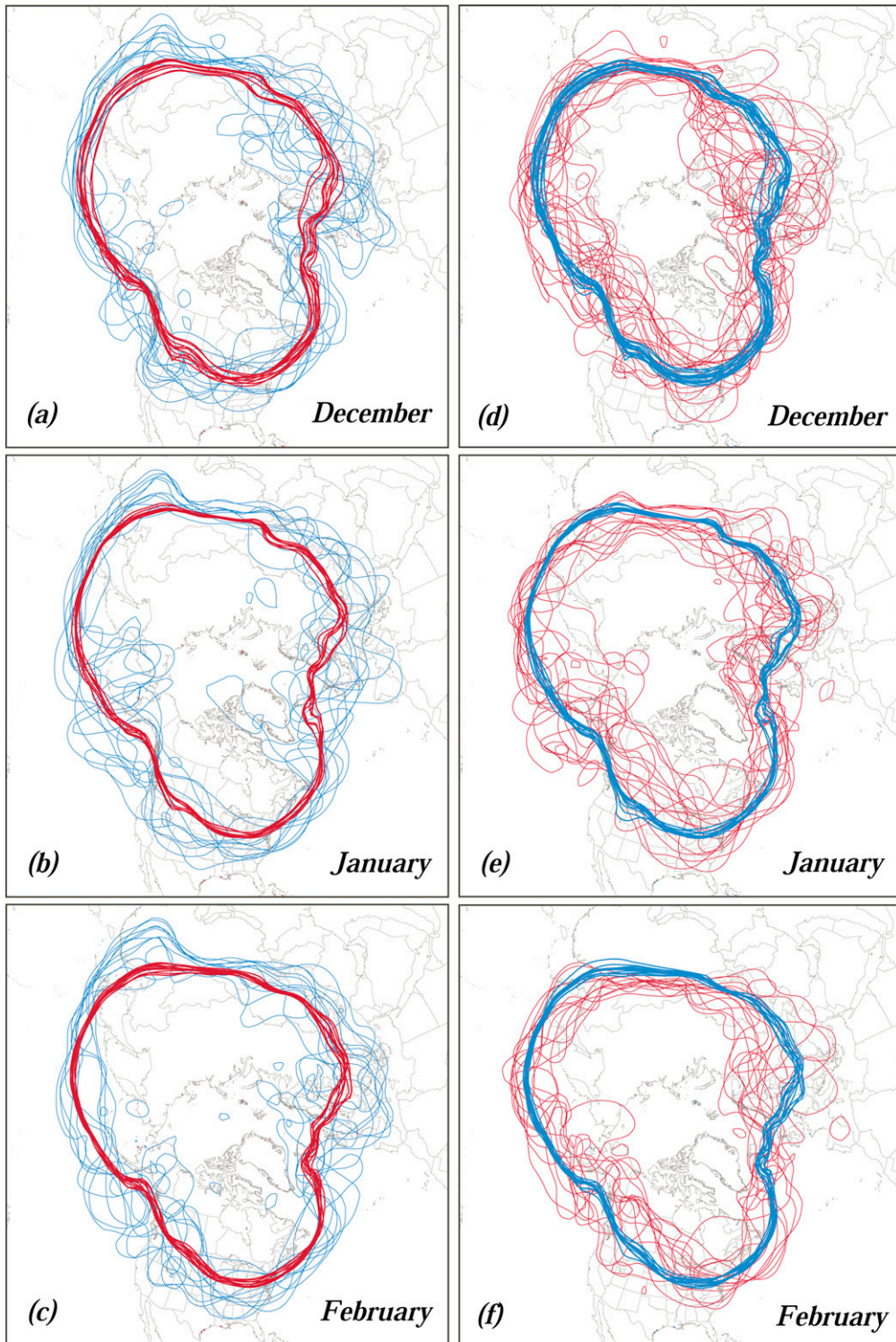


FIG. 9. (a) Blue lines are daily averaged -5°C isotherm on 12 select December days (see text for explanation) when the areal extent of -5°C air was $>2\sigma$ above the 66-yr mean for that day. Thick red lines are the 66-yr daily average -5°C isotherms for those calendar days. (b) As in (a), but for the 11 select days in January. (c) As in (a), but for the 11 select days in February. (d) Red lines are the daily averaged -5°C isotherm on 20 select December days when the areal extent of the -5°C air was $<2\sigma$ below the 66-yr mean for that day. Thick blue lines are the 66-yr daily average -5°C isotherms for those calendar days. (e) As in (d), but for the 15 such days in January. (f) As in (d), but for the 13 select days in February.

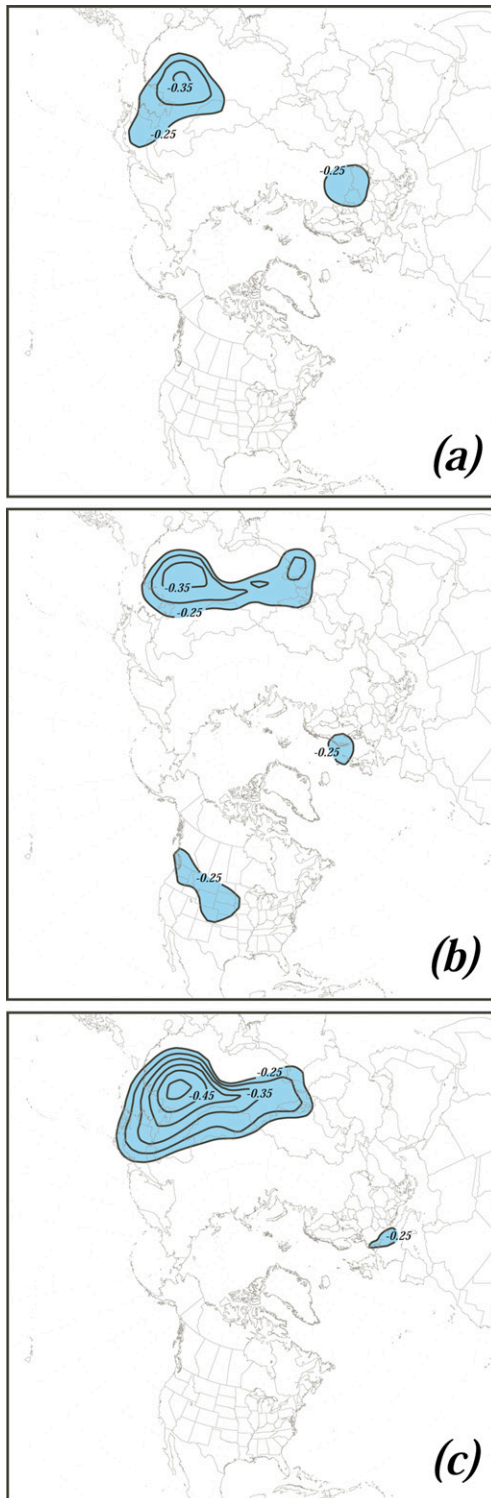


FIG. 10. (a) Map of correlation between the daily average, December, 850-hPa temperature at each grid point (from 1948 to 2013) in the NCEP reanalysis data to the daily time series of normalized Northern Hemisphere cold pool area for each December day in that interval. Magnitudes of correlations significant at the 95% level are contoured and blue shaded every 0.05 beginning at -0.25 . (b) As in (a), but for January days from 1948 to 2014. (c) As in (a), but for February days from 1948 to 2014.

century. Though only results for the Northern Hemisphere have been reported here, similar results were found for the Southern Hemisphere in the course of this work. The rate of contraction of the Northern Hemispheric cold pool is nearly identical to that of the February Arctic sea ice extent (Serreze et al. 2007), a signal regarded as an important diagnostic of climate change.

Angell (2006) examined trends in the size of the DJF 300-hPa circumpolar vortex (CPV) for the period 1963–2001 via consideration of the area enclosed by the 9120-m isohypse at 300 hPa. He found a statistically significant decrease in vortex size that was accompanied by an increase in 850–300-hPa temperature. Employing the NCEP reanalysis data, we extended that analysis (not shown) by calculating the DJF average area of the CPV over the period 1948/49–2013/14 and found that the correlation between the CPV area thus defined and the 850-hPa -5°C cold pool area was 0.455 69. Additionally, the 300-hPa CPV contraction (significant above the 99% level) has been only 80% as fast as that of the 850-hPa cold pool.

Much of the analysis in this paper has focused on the areal extent of the -5°C air at 850 hPa. Superimposed upon the cold pool's steady contraction is considerable interannual variability in both its areal extent and the geographic distribution of the cold air. Employing daily average time series in each of the winter seasons covered by the NCEP reanalysis data, each of the past 66 Northern Hemisphere winter seasons were ranked from coldest (i.e., largest seasonally averaged normalized area) to warmest (smallest seasonally averaged normalized area). Composite differences between the five coldest and five warmest years include much colder 850-hPa temperatures in Eurasia–Siberia and northwestern Canada, a tendency for anomalous midtropospheric ridging over the North Atlantic and Scandinavia, a weaker North Atlantic jet, and a southward-displaced, extended jet in the central Pacific. These composite differences in the Atlantic sector are reminiscent of the negative phase of the Arctic Oscillation (AO) though nearly no correlation exists between the seasonally averaged -5°C cold pool area and the seasonally averaged AO index.

The variability of the cold pool is not uniform across all longitudes. In fact, the greatest interannual variability is found at the end of the Pacific and Atlantic storm tracks. Within these rather limited regions (Fig. 4), nearly $\frac{1}{2}$ of the contraction of the 850-hPa -5°C cold pool has taken place since 1948/49. Whether or not this result is tied to the poleward migration of the storm tracks as the planet warms is a topic for further inquiry. It does suggest, however, that, to the extent that long-term contraction of the cold pool is tied to subtle large-scale

circulation changes, those changes are nonuniformly distributed across the hemisphere.

A cursory comparison of the distribution of -5°C air on winter days with large and small cold pool areas (defined as days with standardized anomalies in area >2.0 or <-2.0) revealed cold air in central China as a ubiquitous, and nearly exclusive, characteristic of hemispheric extreme cold events. This observation hints at the role the East Asian winter monsoon (EAWM) may play in the interannual hemispheric variability of the 850-hPa cold pool. Jaffe et al. (2011) found that the EAWM index of Jhun and Lee (2004), which focuses on the meridional shear of the 300-hPa wind near the Pacific jet entrance region, was significantly correlated with the rapid decrease in wind speed at the Pacific jet exit region that characterized what Jaffe et al. (2011) termed jet retraction. Specifically, jet retraction events appear to be strongly related to break periods in the EAWM. Analyses presented here (Figs. 8, 9) conversely suggest that cold surges into central China (Figs. 9a–c), characteristic of hemispheric cold events, may be associated with extended Pacific jets (Fig. 8c). A recent study by Wang and Chen (2014) introduces a new intensity index for the EAWM that incorporates both north–south and east–west sea level pressure (SLP) gradients. Using this index they identified 16 strong EAWM winters (i.e., those characterized by numerous, intense cold surges off the coast of China). Of those 16, 11 were in the top 17 coldest winters as measured by the normalized -5°C cold pool area (Fig. 2). Thus, nearly $2/3$ of the coldest quartile of winters since 1948 have been characterized by a strong EAWM. Despite this intriguing relationship, the correlation between the seasonally averaged, -5°C cold pool area and the Wang and Chen (2014) EAWM index is small (0.277). A similarly meager correlation (0.2369) exists between the seasonally averaged cold pool area and the seasonally averaged Siberian high index (SHI)¹⁰ first proposed by Gong and Ho (2002). Though both of these correlations are small, they are notably larger than the correlations to other global-scale phenomena reported earlier. Thus, the nature of this possible physical connection as well as its consequences for hemispheric circulation changes is the topic of ongoing research. To identify characteristic precursor disturbances and describe their synoptic evolutions, a necessary component of this work will be the examination of case studies of substantial intraseasonal cold pool expansions characterized by a cold central China.

¹⁰ The SHI is the average sea level pressure over the region 40° – 60°N and 70° – 120°E . It was calculated using the NCEP reanalysis data over the entire 66-yr time series.

Finally, extension of the cold pool analysis described here to output from the suite of climate models employed in phase 5 of the Climate Model Intercomparison Project (CMIP5), also currently underway, offers a straightforward way to diagnose the component model's performances with respect to reanalysis depictions of both the long-term and interannual cold pool variability. Employing simulations from the models that demonstrate the greatest fidelity to the reanalyses would permit confident consideration of future projections of lower-tropospheric temperature trends and associated circulation anomalies. In fact, employing such model output, it would be feasible to extend the analysis method described here to three dimensions in order to consider long-term trends in the masses of free tropospheric air cooled to certain potential temperatures during winter. Such an analysis would then directly convert the mass differences to energy differences allowing for more precise comparison to other independent calculations of changes in Earth's energy budget.

Acknowledgments. This work was supported by the National Science Foundation through Grant NSF-1265182. The author is grateful for the thoughtful and constructive reviews of three reviewers.

REFERENCES

- Angell, J. K., 2006: Changes in the 300-mb north circumpolar vortex, 1963–2001. *J. Climate*, **19**, 2984–2994, doi:10.1175/JCLI3778.1.
- Brohan, P., J. J. Kennedy, I. Harris, S. F. B. Tett, and P. D. Jones, 2006: Uncertainty estimates in regional and global observed temperature changes: A new data set from 1850. *J. Geophys. Res.*, **111**, D12106, doi:10.1029/2005JD006548.
- Brown, R. D., 2000: Northern Hemisphere snow cover variability and change, 1915–97. *J. Climate*, **13**, 2339–2355, doi:10.1175/1520-0442(2000)013<2339:NHSCVA>2.0.CO;2.
- Chu, P.-S., A. J. Nash, and F.-Y. Porter, 1993: Diagnostic studies of two contrasting rainfall episodes in Hawaii: Dry 1981 and wet 1982. *J. Climate*, **6**, 1457–1462, doi:10.1175/1520-0442(1993)006<1457:DSOTCR>2.0.CO;2.
- Cohen, J., and D. Entekhabi, 1999: Eurasian snow cover variability and Northern Hemisphere climate predictability. *Geophys. Res. Lett.*, **26**, 345–348, doi:10.1029/1998GL900321.
- Foster, J., M. Owe, and A. Rango, 1983: Snow cover and temperature relationships in North America and Eurasia. *J. Climate Appl. Meteor.*, **22**, 460–469, doi:10.1175/1520-0450(1983)022<0460:SCATRI>2.0.CO;2.
- Gong, D.-Y., and C.-H. Ho, 2002: The Siberian high and climate change over middle to high latitude Asia. *Theor. Appl. Climatol.*, **72**, 1–9, doi:10.1007/s007040200008.
- Hansen, J., R. Ruedy, M. Sato, M. Imhoff, W. Lawrence, D. Easterling, T. Peterson, and T. Karl, 2001: A closer look at United States and global surface temperature change. *J. Geophys. Res.*, **106**, 23 947–23 963, doi:10.1029/2001JD000354.
- , —, —, and K. Lo, 2010: Global surface temperature change. *Rev. Geophys.*, **48**, RG4004, doi:10.1029/2010RG000345.

- Jaffe, S. C., J. E. Martin, D. J. Vimont, and D. J. Lorenz, 2011: A synoptic climatology of episodic, subseasonal retractions of the Pacific jet. *J. Climate*, **24**, 2846–2860, doi:10.1175/2010JCLI3995.1.
- Jhun, J.-G., and E.-J. Lee, 2004: A new East Asian winter monsoon index and associated characteristics of the winter monsoon. *J. Climate*, **17**, 711–726, doi:10.1175/1520-0442(2004)017<0711:ANEAWM>2.0.CO;2.
- Kalnay, E., and Coauthors, 1996: The NCEP/NCAR 40-Year Reanalysis Project. *Bull. Amer. Meteor. Soc.*, **77**, 437–471, doi:10.1175/1520-0477(1996)077<0437:TNYRP>2.0.CO;2.
- Karl, T. R., S. J. Hassol, C. D. Miller, and W. L. Murray, Eds., 2006: Temperature trends in the lower atmosphere: Steps for understanding and reconciling differences. U.S. Climate Change Science Program and the Subcommittee on Global Change Research Rep., 164 pp. [Available online at <http://data.globalchange.gov/assets/51/56/6d7da49e1f93bef673d56ff6aa6a/sap1-1-final-all.pdf>.]
- Lawrimore, J., M. Menne, B. Gleason, C. Williams Jr., D. Wuertz, R. Vose, and J. Rennie, 2011: An overview of the Global Historical Climatology Network monthly mean temperature dataset, version 3. *J. Geophys. Res.*, **116**, D19121, doi:10.1029/2011JD016187.
- Lugina, K. M., P. Ya. Groisman, K. Y. Vinnikov, V. V. Koknaeva, and N. A. Speranskaya, 2005: Monthly surface air temperature time series area-averaged over the 30-degree latitudinal belts of the globe, 1881–2005. Carbon Dioxide Information Analysis Center, Oak Ridge National Laboratory, U.S. Department of Energy, doi:10.3334/CDIAC/cli.003.
- Magnuson, J. J., and Coauthors, 2000: Historical trends in lake and river ice cover in the Northern Hemisphere. *Science*, **289**, 1743–1746, doi:10.1126/science.289.5485.1743.
- Morice, C. P., J. J. Kennedy, N. A. Rayner, and P. D. Jones, 2012: Quantifying uncertainties in global and regional temperature change using an ensemble of observational estimates: The HadCRUT4 dataset. *J. Geophys. Res.*, **117**, D08101, doi:10.1029/2011JD017187.
- Przybylak, R., 2007: Recent air-temperature changes in the Arctic. *Ann. Glaciol.*, **46**, 316–324, doi:10.3189/172756407782871666.
- Saha, S., and Coauthors, 2010: The NCEP Climate Forecast System Reanalysis. *Bull. Amer. Meteor. Soc.*, **91**, 1015–1057, doi:10.1175/2010BAMS3001.1.
- Scruggs, L., and S. Benegal, 2012: Declining public concern about climate change: Can we blame the great recession? *Global Environ. Change*, **22**, 505–515, doi:10.1016/j.gloenvcha.2012.01.002.
- Serreze, M., M. M. Holland, and J. Stroeve, 2007: Perspectives on the Arctic's shrinking sea-ice cover. *Science*, **315**, 1533–1536, doi:10.1126/science.1139426.
- Smith, T. M., and R. W. Reynolds, 2005: A global merged land air and sea surface temperature reconstruction based on historical observations (1880–1997). *J. Climate*, **18**, 2021–2036, doi:10.1175/JCLI3362.1.
- , T. C. Peterson, J. H. Lawrimore, and R. W. Reynolds, 2005: New surface temperature analyses for climate monitoring. *Geophys. Res. Lett.*, **32**, L14712, doi:10.1029/2005GL023402.
- Stocker, T. F., and Coauthors, Eds., 2014: *Climate Change 2013: The Physical Science Basis*. Cambridge University Press, 1535 pp.
- Thompson, D. W. J., and J. M. Wallace, 1998: The Arctic Oscillation signature in the wintertime geopotential height and temperature fields. *Geophys. Res. Lett.*, **25**, 1297–1300, doi:10.1029/98GL00950.
- Uppala, S. M., and Coauthors, 2005: The ERA-40 re-analysis. *Quart. J. Roy. Meteor. Soc.*, **131**, 2961–3012, doi:10.1256/qj.04.176.
- Wang, L., and W. Chen, 2014: An intensity index for the East Asian winter monsoon. *J. Climate*, **27**, 2361–2374, doi:10.1175/JCLI-D-13-00086.1.
- Wang, X. L., V. R. Swail, and F. W. Zwiers, 2006: Climatology and changes of extratropical cyclone activity: Comparison of ERA-40 with NCEP–NCAR reanalysis for 1958–2001. *J. Climate*, **19**, 3145–3166, doi:10.1175/JCLI3781.1.
- Wolter, K., and M. S. Timlin, 1993: Monitoring ENSO in COADS with a seasonally adjusted principal component index. *Proc. 17th Climate Diagnostics Workshop*, Norman, OK, NOAA/NMC/CAC, 52–57.
- Wu, Y., M. Ting, R. Seager, H.-P. Huang, and M. A. Cane, 2010: Changes in storm tracks and energy transports in a warmer climate simulated by the GFDL CM2.1 model. *Climate Dyn.*, **37**, 53–72, doi:10.1007/s00382-010-0776-4.